Effect of Unstable Particle Production on Scattering Amplitudes*

JAMES S. BALL

University of California, Los Angeles, California

AND

PETER THURNAUER†

University of California, San Diego, La Jolla, California

The model for pion-nucleon scattering proposed by Ball, Frazer, and Nauenberg is solved numerically. This model yields unitary scattering amplitudes while including the effects of ρ-meson production and the associated anomalous thresholds. The behavior of the solutions as a function of the width of the ρ meson and the pion-nucleon coupling constant is investigated. Cusps as well as broad peaks are generated in the elastic-scattering amplitude by the ρ-meson production. The effects of the complex singularities are investigated in detail by comparison with another treatment of pion-nucleon scattering in which anomalous cuts are absent. Also, the existence of poles on unphysical sheets is studied by means of a simplified model.

I. INTRODUCTION

AS the analytic structure of two-body scattering amplitudes has become increasingly well understood and exploited in recent years, it has become apparent that even at low energies these amplitudes may be strongly affected by the inelastic production of low-mass multiparticle states. There seems to be some experimental as well as theoretical justification for assuming that these production processes may be dominantly the production of a two-particle state in which one or both of the particles are unstable and subsequently decay, producing the multiparticle final state. A procedure by which scattering and production of unstable particles may be treated has been developed by Ball, Frazer, and Nauenberg[1]; in particular, these authors have constructed a model for pion-nucleon scattering in which the effects of the production of a pion are included. The complexity of the three-body states is reduced by treating the two pions as an unstable ρ resonance. This model satisfies the unitarity requirements for all three processes $\pi + N \rightarrow \pi + N$, $\pi + N \rightarrow \rho + N$, and $\rho + N \rightarrow \rho + N$ by having the appropriate discontinuities for the scattering amplitudes in both total energy and energy of the two pions forming a ρ. At the same time, the longest range interaction in the $\pi + N \rightarrow \rho + N$ channel, namely one-pion exchange, is included. To preserve the conditions demanded by unitarity, which is the main task BFN impose upon themselves, it is necessary as well to add nucleon pole contributions to the one-pion-exchange approximation. The end result of BFN is a linear integral equation whose solution allows the calculation of the various scattering amplitudes by quadrature. The main difficulty in carrying out this program lies in the evaluation of the kernel of the integral equation

which requires a numerical integration over complex singularities arising from the anomalous thresholds present in this process.

The purpose of this paper is to report on the results obtained by carrying out the computational procedure formulated in BFN and to discuss the physical implications of these results. While the main interest in performing this calculation was as an intermediate step prior to doing the physical $\pi N \rightarrow \rho N$ problem, the simpler model of BFN affords a better opportunity for an investigation of the scattering amplitudes unhampered by inessential complications of spin. Of particular interest is the effect of the complex singularities on the scattering amplitudes, especially in the region near the ρ-nucleon threshold. Also, the familiar cusplike behavior in the cross section at the inelastic threshold[2,3] and its dependence on the pion-nucleon coupling constant as well as the width of the ρ can be studied. Finally, an attempt can be made to understand the underlying analytic structure of the solutions obtained as well as their self-consistency.

In Sec. II, we give an outline of the calculation, which is essentially a recapitulation of the relevant parts of BFN. Section III lists the main results of the calculation for various values of the parameters involved. We also present an interpretation of the results with the aid of a simplified version of the BFN model.

II. OUTLINE AND DETAILS OF THE CALCULATION

While the conventions of BFN will be used consistently throughout this paper, we nevertheless list here the assumptions and definitions given in BFN that are directly pertinent to our calculation. In the interests of simplicity, all spins and isotopic spins have been neglected, including those of the ρ resonance, and only S-wave scattering for all channels has been considered. The amplitudes for the processes $\pi N \rightarrow \pi N$, $\pi N \rightarrow \rho N$, $\rho N \rightarrow \rho N$ are given by $T_{11}(s,t)$, $T_{21}(s,t,\omega)$, $T_{22}(s,t,\omega,\omega')$,

[1] J. S. Ball, W. R. Frazer, and M. Nauenberg, Phys. Rev. 128, 478 (1962). We refer to this work hereafter as BFN.

[2] M. Nauenberg and A. Pais, Phys. Rev. 126, 360 (1962).

[3] J. S. Ball and W. R. Frazer, Phys. Rev. Letters 7, 204 (1961)

respectively, where s designates the usual square of the center-of-mass energy, t the invariant momentum transfer, and ω is the square of the energy of the two final resonant pions of T_{21} and T_{22} in their center-of-mass frame, while ω' is the same for the two initial pions of T_{22}.

Amplitudes M_{11}, M_{12}, M_{21}, and M_{22}, which are slowly varying functions of ω and ω', can then be formed by factoring out the initial- and final-state interactions between the pion pairs as follows:

$$M_{11}(s,t)=T_{11}(s,t), \qquad (2.1a)$$

$$M_{21}(s,t,\omega)=T_{21}(s,t,\omega)/f(\omega)=M_{12}(s,t,\omega), \quad (2.1b)$$

$$M_{22}(s,t,\omega,\omega')=T_{22}{}^c(s,t,\omega,\omega')/f(\omega)f(\omega'), \qquad (2.1c)$$

where $f(\omega)$ is the S-wave pion-pion scattering amplitude

$$f(\omega)=16\pi[\omega/(\omega-4\mu^2)]^{1/2}e^{i\delta(\omega)}\sin\delta(\omega)$$

and $T_{22}{}^c$ refers to "connected" scattering processes.[4] If we now specialize to the case $\omega=\omega'=m_\rho{}^2$, where $m_\rho(\approx 5.4\,\mu)$ is the physical mass of the ρ meson, the functions M can then be written in terms of 2×2 n and d matrices:

$$M=n(I+d)^{-1}. \qquad (2.2)$$

The particular choice of n and d made by BFN leads to the following linear integral equations:

$$n_{21}(s)=B(s)+\int_{(M+2\mu)^2}^{\infty}ds'\rho_2(s_+')L(s,s')n_{21}(s'), \qquad (2.3a)$$

$$n_{22}(s)=\bar{B}(s)+\int_{(M+2\mu)^2}^{\infty}ds'\rho_2(s_+')L(s,s')n_{22}(s'). \qquad (2.3b)$$

These equations have the virtue that they contain only real functions and the integral is evaluated over a real contour. All of the complexity due to the anomalous thresholds is now contained in the kernel $L(s,s')$. The remaining n's and d's can then be obtained by quadrature as follows:

$$n_{11}(s)=\int_{(M+2\mu)^2}^{\infty}ds'\rho_2(s_+')K(s,s')n_{21}(s'), \qquad (2.4a)$$

$$n_{12}(s)=B(s)+\int_{(M+2\mu)^2}^{\infty}ds'\rho_2(s_+')K(s,s')n_{22}(s'), \qquad (2.4b)$$

$$d_{11}(s)=-\frac{i}{\pi}\int_C ds'\frac{\rho_1(s')\alpha(s')d_{21}(s')}{s'-s}$$
$$-\frac{1}{\pi}\int_{(M+\mu)^2}^{\infty}ds'\frac{\rho_1(s_+')n_{11}(s')}{s'-s}, \qquad (2.4c)$$

$$d_{12}(s)=-\frac{i}{\pi}\int_C ds'\frac{\rho_1(s')\alpha(s')[1+d_{22}(s')]}{s'-s}$$
$$-\frac{1}{\pi}\int_{(M+\mu)^2}^{\infty}ds'\frac{\rho_1(s_+')n_{12}(s')}{s'-s}, \qquad (2.4d)$$

$$d_{21}(s)=-\frac{1}{\pi}\int_{(M+2\mu)^2}^{\infty}ds'\frac{\rho_2(s_+')n_{21}(s')}{s'-s}, \qquad (2.4e)$$

$$d_{22}(s)=-\frac{1}{\pi}\int_{(M+2\mu)^2}^{\infty}ds'\frac{\rho_2(s_+')n_{22}(s')}{s'-s}, \qquad (2.4f)$$

where the kernel of the integral equation is

$$L(s,s')=\int_{(M+\mu)^2}^{\infty}ds''\rho_1(s_+'')K(s,s'')K(s',s'')$$
$$+\frac{i}{\pi}\int_C ds''\rho_1(s'')\alpha(s'')\left[\frac{K(s_+'',s')}{s''-s}\right.$$
$$\left.+\frac{K(s_+'',s)}{s''-s}-\frac{2i\alpha(s'')}{\pi(s''-s)(s''-s')}\right], \qquad (2.5a)$$

$$K(s,s')=\frac{B(s)-B(s')}{\pi(s-s')}, \qquad (2.5b)$$

and $B(s)$ is the S-wave projection of the one-pion-exchange pole term, given by

$$B(s)=\frac{\alpha(s)}{\pi}\ln\left[\frac{\alpha(s)+\beta(s)}{\alpha(s)-\beta(s)}\right], \qquad (2.6)$$

and

$$\bar{B}(s)=\int_{(M+\mu)^2}^{\infty}ds'\rho_1(s')K(s,s')B(s')+\frac{i}{\pi}\int_C\frac{\alpha(s')\rho_1(s')}{s'-s}[2B(s_+')-B(s)-2i\alpha(s')], \qquad (2.7)$$

$$\alpha(s)=\frac{\pi sg}{\{[s-(M+\mu)^2][s-(M-\mu)^2][s-(M-m_\rho)^2][s-(M+m_\rho)^2]\}^{1/2}}, \qquad (2.8a)$$

$$\beta(s)=\frac{\pi sg}{s^2-s(2M^2+m_\rho{}^2-\mu^2)+(M^2-\mu^2)(M^2-m_\rho{}^2)}, \qquad (2.8b)$$

$$\rho_1(s)=\frac{\{[s-(M+\mu)^2][s-(M-\mu)^2]\}^{1/2}}{16\pi s}, \qquad (2.8c)$$

---

[4] See Sec. II of BFN.

$$\rho_2(s) = \int_{4\mu^2}^{(s^{1/2}-M)^2} d\omega' \frac{\{[s-(M+\sqrt{\omega'})^2][s-(M-\omega'^{1/2})^2]\}^{1/2}}{128\pi^3 s} \left[\frac{\omega'-4\mu^2}{\omega'}\right] |f(\omega')|^2, \tag{2.8d}$$

where M and μ are the masses of the nucleon and pion, respectively, and g is the pion-nucleon coupling constant. The subscript $+$ on the variable s as it appears in the foregoing equations implies that s is to be taken at its limiting values just above the various cuts involved. The precise definition of this procedure is given in BFN. We represent the pion-pion scattering amplitude $f(\omega)$ by a Breit-Wigner formula in the following manner:

$$f(\omega) = 16\pi[\omega/(\omega-4\mu^2)]^{1/2}$$

$$\times \frac{(\gamma/2)[(\omega-4\mu^2)/\omega]^{1/2}}{m_\rho^2-\omega-i(\gamma/2)[(\omega-4\mu^2)/\omega]^{1/2}}, \tag{2.9}$$

in which γ is related to the half-width of the ρ meson on the $\omega^{1/2}$ scale by

$$\gamma_{1/2} = (\gamma/4m_\rho)[(m_\rho^2-4\mu^2)/m_\rho^2]^{1/2}. \tag{2.10}$$

Finally, the complex contour C goes from s_- to s_+ where

$$s_\pm = M^2+\tfrac{1}{2}m_\rho^2 \mp i(m_\rho/2\mu)[(4M^2-\mu^2)(m_\rho^2-4\mu^2)]^{1/2}$$

$$= 59.39\,\mu^2 \mp 179.89i\,\mu^2, \tag{2.11}$$

and C may cross the real axis at any point between $(M+\mu)^2$ and $(M+m_\rho)^2$. In integrals in which the integrand has a cut in that region, the contour is split into two parts, such that one segment goes from s_- to a limiting point just above the cut and the other from a limiting point just below the cut to s_+.

The first step in solving the n and d equations is to calculate the kernel $L(s,s')$ for real values of $s,s' > (M+2\mu)^2$. This is probably the most difficult part of the BFN program, as it requires a numerical integration over complex singularities arising from the anomalous

thresholds present in the problem. Once the kernel is known, Eqs. (2.3a) and (2.3b) can be solved numerically by a matrix inversion procedure yielding n_{21} and n_{22}. The other n's and d's follow directly from Eqs. (2.4), and the scattering amplitudes can then be obtained. We have carried out this somewhat lengthy, but straightforward procedure, and the results are presented in the following section.

III. RESULTS AND THEIR INTERPRETATION

The results obtained for the pion-nucleon elastic- and inelastic-scattering amplitudes are shown in Figs. 2, 3, and 4. Actually, what has been plotted are the squares of scattering amplitudes times appropriate phase space factors, so that the unitarity limit for the elastic channel is 1, while that for the inelastic channel is 0.25. It can be seen that increasing the pion-nucleon coupling constant causes cusps to grow until they finally become rather flat and near the unitarity limit below the second threshold but fall off fairly rapidly above that point. As the width of the ρ resonance is increased, the cusps become more rounded or "woollier," but the same general trend of growth and loss of symmetric shape with increased pion-nucleon coupling can be noted.

Figure 5 shows the departure of T_{21} satisfying unitarity from the Born approximation for T_{21} denoted by B_{21}. In the energy region where the Born term is small compared to the unitarity limit the rise of B_{21} is closely matched by that of T_{21} as had been conjectured by Ball and Frazer.[3] Also, for values of the coupling constant such that B_{21} is near the unitarity limit the shapes of B_{21} and T_{21} are quite similar; however, for larger coupling constants when B_{21} is an order of magnitude above the unitarity limit the shape of T_{21} differs from that of B_{21} in having a slower rise and a maximum at higher energy.

In Fig. 6, we have plotted the real and imaginary

FIG. 1. The contour C in the s plane for $\omega=m_\rho^2 \approx 29$.
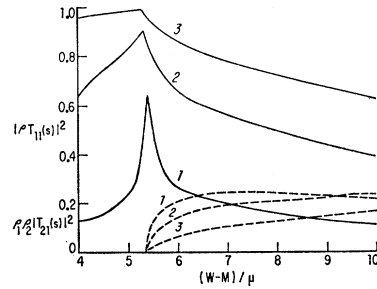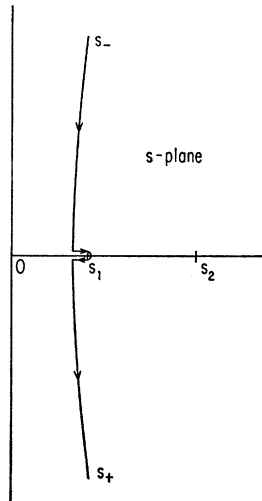
FIG. 2. The solid curves 1, 2, 3 give the elastic scattering amplitudes squared for increasing values of the π-N coupling constant in the BFN model. The dashed curves are the corresponding inelastic amplitudes. The quantity $W=s^{1/2}$ and the width of the ρ resonance is very small: $\gamma=0.1\mu^2$. The top curve decreases only very slowly as it extends left towards the first threshold.
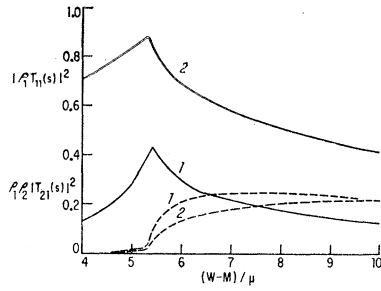
FIG. 3. The elastic and inelastic scattering amplitudes squared for increasing values of the π-N coupling constant. The ρ-resonance width is now $\gamma = 1.0\,\mu^2$, and the effect of this larger width may be seen in the more rounded cusps as well as in the more gradual appearance of the inelastic channel.

parts of the determinant of the d's,

$$D = [(1+d_{11})(1+d_{22}) - d_{12}d_{21}],$$

which appears as a factor in the denominator for the scattering amplitudes $\pi N \to \pi N$, $\pi N \to \rho N$, $\rho N \to \rho N$. The real part of D is remarkably flat between s_1 and s_2, and this behavior is reflected in the flatness of the elastic scattering amplitude for certain values of g, as we have already seen. We shall discuss this remarkable behavior of D later in the section with the aid of a simplified model. Finally, the D function, which rises smoothly to its asymptotic value of 1 at $s = -\infty$, has no zeros in the unphysical regions of the s plane, at least for interesting values of the pion-nucleon coupling constant. Figure 6 shows this to be true along the real
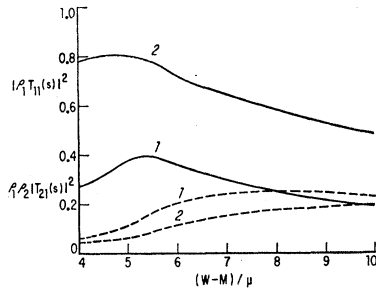
FIG. 4. The elastic and inelastic amplitudes for increasing g, but with ρ-resonance width large: $\gamma = 10.0\,\mu^2$. The increased "woolly" effects of a wide ρ-resonance width can be clearly seen.

axis below the first threshold, and one may check the rest of s plane using the well-known "principle of the argument" theorem.[5] Thus, the BFN model is seen to be self-consistent in so far as the scattering amplitudes contain no spurious singularities, or "ghosts," which often plague solutions to this type of problem.[6]

---

[5] See, for example, E. T. Copson, *An Introduction to the Theory of Functions of a Complex Variable* (Oxford University Press, Oxford, England, 1955), p. 119.

[6] It is well known that ghost poles are produced in the calculation of one channel partial-wave scattering amplitudes by the N/D method when the interaction is sufficiently repulsive. In two-channel scattering processes with an interaction only in the

To try to estimate the effect of the complex singularities on the scattering amplitudes, we also solved the following variation of the BFN model. Instead of taking the one-pion exchange as the dynamical input, we exchanged a particle having the mass of the ω. With this heavier particle, there is no anomalous threshold, and hence there are no complex singularities. Using this interaction, we varied the coupling constant and compared the solutions with those obtained in the one-pion-exchange model. For small values of coupling, the behavior of these solutions is similar to that obtained with the pion-exchange interaction in that a small cusp
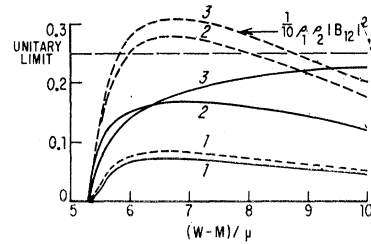
FIG. 5. The solid curves 1, 2, 3 are the inelastic scattering amplitudes squared for increasing values of the π-N coupling constant. The dashed curves give the corresponding Born terms squared. The ρ width is constant at $\gamma = 0.1\,\mu^2$. Note that the inelastic amplitudes remain below the unitarity limit.

appears at the ρ-production threshold and the production amplitude increases with increasing coupling constant. However, above a critical value of coupling the behavior of this solution departs radically from the pion-exchange solution. The elastic channel (T_{11}) cusp moves toward lower energy becoming a resonance, while the production amplitude T_{21}, which contains the only interaction terms, decreases with increasing coupling, becoming negligibly small for very large coupling.

To illustrate the difference between these solutions, we have taken the ω coupling large enough to produce
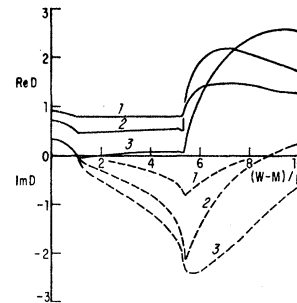
FIG. 6. The solid curves give the real and the dashed curves the imaginary parts of the D function in the BFN model. The labels 1, 2, 3 refer to results obtained for increasing values of the π-N coupling constant. For these curves $\gamma = 0.1\,\mu^2$.

---

off-diagonal channel, which would usually be considered an attractive interaction for the two elastic amplitudes, ghosts can also appear. An example of a solution to a two-channel problem containing a ghost pole occurs in the work of L. F. Cook and B. W. Lee, Phys. Rev. **127**, 297 (1962).
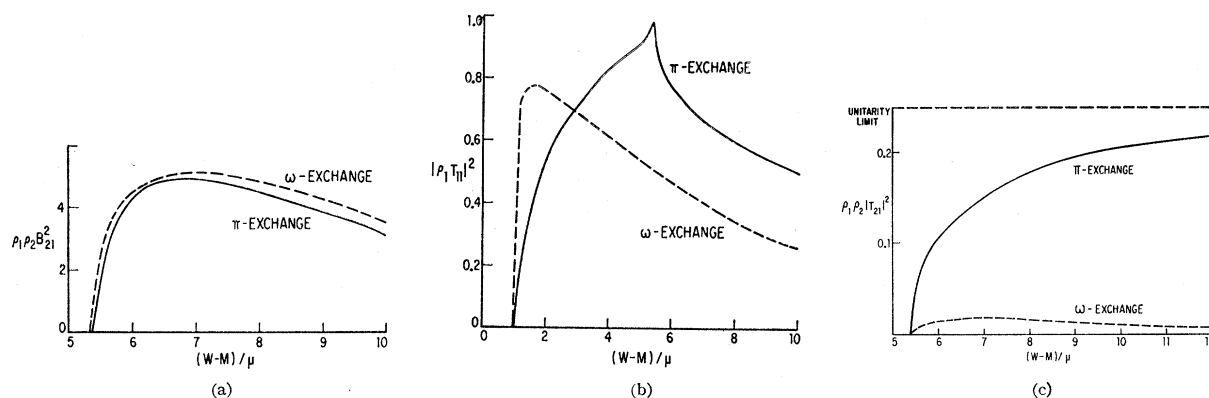
FIG. 7(a) The Born terms squared for the π- and ω-exchange versions of the BFN model. The coupling constants have been chosen so that the Born terms are roughly the same in the low-energy physical region. (b) The scattering amplitudes squared corresponding to the Born terms of Fig. 7(a). For the cases shown here, the ω-exchange model has already developed a ghost pole, while the π-exchange model does not contain a ghost. (c) The corresponding inelastic scattering amplitudes squared for the Born terms of Fig. 7(a). Note that the ghost-containing, ω-exchange, inelastic amplitude is significantly smaller than that of the π-exchange model.

a resonance, and for the sake of comparison, we have adjusted the pion-exchange coupling so that the input Born terms for both solutions are nearly equal in the low energy region as shown in Fig. 7(a). In Fig. 7(b) we show the T_{11} and T_{21} amplitudes for each input Born term. The striking difference between these solutions is due to a "ghost" pole which appears as a zero in the D function for the ω-exchange model at the critical value of the coupling constant and moves to the right as the coupling constant is increased. Once this "ghost" pole appears, the physical significance of the solution is doubtful, since the solution then contains an interaction pole in each channel of entirely mathematical origin and without any physical basis. As has been pointed out, the pion-exchange model contains additional interactions required by unitarity of the two-pion final state, and these interaction terms in T_{21} and T_{22}, together with the complex singularities, provide enough additional interaction to allow the ND^{-1} equation to satisfy unitarity without producing a spurious singularity. Thus, unitarity is maintained with only interaction terms of physical origin. These results indicate that great care must be exercised in any approximation scheme to low-mass exchange which ignores the complications of complex singularities.

The precise origin of the shape and size of the curves presented in Figs. 2–4 can, in principle, be found from a thorough investigation of the analytic properties of the scattering amplitudes as a function of s. Unfortunately, our model is already too complicated for practicable ventures into unphysical Riemann sheets, but an approximate BFN model, which produces results similar to the original, does allow for easy excursions away from the physical cut. This approximation is made by replacing the left-hand partial-wave singularities of the inelastic channel in the BFN model by a single pole and also taking the ρ to be a stable particle. We shall refer to this simplified version of BFN as the single-pole approximation.

With this pole approximation the elastic scattering amplitude T_{11} becomes

$$T_{11} = R^2(U_2 - W_2)/(s - s_0)D, \qquad (3.1)$$

where

$$D = 1 - R^2(U_1 - W_1)(U_2 - W_2),$$

$$W_i(s) = -\frac{1}{\pi} \int_{s_i}^{\infty} ds' \frac{\rho_i(s')}{(s' - s)(s' - s_0)}, \quad i = 1,2 \quad (3.2)$$

$$U_i = W_i(s_0);$$

s_1 is the position of the first threshold, and s_2 that of the second. The kinematic functions ρ_i are essentially the same as those of BFN, namely,

$$\rho_i = \frac{1}{16\pi} \frac{\{[s - (M - m_i)^2][s - (M + m_i)^2]\}^{1/2}}{s}, \quad i = 1,2 \qquad (3.3)$$

with $m_1 = \mu$, $m_2 = m_\rho$, but unlike BFN the form of ρ_2 has been taken here to correspond to the fact that the ρ
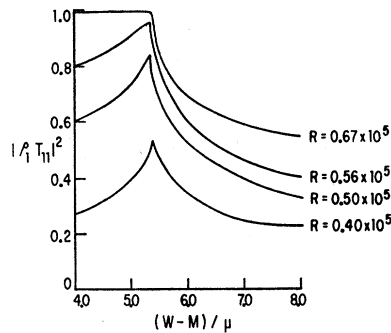
FIG. 8. The elastic scattering amplitudes squared in the single-pole approximation with stable ρ meson. The values of the residue of the interaction pole appropriate to each curve are shown. The pole position is at $s_0 = -500 \mu^2$. The top curve remains virtually constant down to the first threshold.
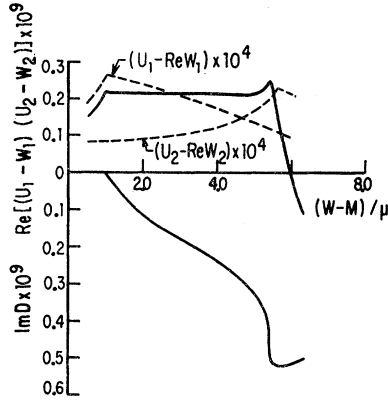
FIG. 9. The lower solid curve is the imaginary part of the D function in the single-pole approximation. The upper solid curve is a term which enters into the real part of $D=1-R^2(U_1-W_1)(U_2-W_2)$, and the dashed curves are the single-channel contributions to this term. Note that each single-channel curve has a cusp at its respective threshold, and the resultant product curve is hence fairly constant between the two thresholds.

meson is now stable. R is the residue of the interaction pole, while s_0 is its position. In this model a ghost pole will appear at $s=-\infty$ when $R^2=1/(U_1 U_2)$ and continue to move to the right as R is increased. The limiting position of the ghost pole with large R, however, is s_0.

The values of the scattering amplitude which are obtained in this model are shown in Fig. 8. It can be seen that the curves resemble those obtained with the BFN model and develop in a similar way with increasing R. In particular, the top curve is virtually constant between s_1 and s_2, as likewise occurred for the preceding model. The interaction pole position is at $s_0=-500\ \mu^2$, this point having been chosen because of the close similarity of the results with those found in our calculation of the BFN model. In Fig. 9, we plot what are essentially the real and imaginary parts of the D function in the single-pole approximation. The single-channel contributions are also shown, and it may be noted that it is their product which leads to the virtual constancy of Re D between s_1 and s_2, which we have already seen in the BFN model (see Fig. 6).

In order to understand the shapes obtained for the physical scattering amplitude in Fig. 8 and, in particular, the rather curious flat curves near the unitarity limit for certain values of R, one must study the analytic behavior of this function in the nearby unphysical regions of the s plane. This is done in the Appendix. It is found there that a pole whose position varys with R moves close to the region of s_1 to s_2 for values of R corresponding to the top curve in Fig. 8. The nearby pole not only causes the scattering amplitude to rise towards its unitarity limit in the immediate vicinity of the pole, but also, because of the flat behavior of the D function, can communicate this effect on the scattering amplitude throughout the region from s_1 to s_2. The result is that the scattering amplitude is nearly constant and

close to its unitarity limit between s_1 and s_2 for these values of R.

The same argument can be applied to the results obtained for the BFN model. The behavior of Re D as shown in Fig. 6 can be traced to the scattering amplitudes' having S-wave thresholds at both s_1 and s_2. Since each term of D is the product of two functions, one with a cusp at s_1 and the other with a cusp at s_2, the resulting D function will tend to be relatively flat between these two cusps provided the maxima of D at s_1 and s_2 are about equal. A nearby pole in the scattering amplitude will necessarily emphasize this effect. We also expect that if the threshold behavior at s_1 were that of a partial wave with $l>0$, the cusp-like phenomenon at s_2 would become dominant, producing a resonance behavior below s_2 for sufficiently large coupling constant, as occurred, for example, in the work of Frazer and Hendry.[7]

ACKNOWLEDGMENT

APPENDIX

In the single-pole approximation to two-channel stable-particle scattering with an interaction pole of residue R and position s_0 in the off-diagonal channel, a common factor in the denominators of the scattering amplitudes T_{11}, T_{21}, and T_{22} is

$$D=1-R^2(U_1-W_1)(U_2-W_2), \qquad (A1)$$

where the various quantities given in the above equation are defined in Eq. (3.2). The W_i may be written as

$$W_i(s)=[V_i(s)-V_i(s_0)]/[s-s_0], \qquad (A2)$$

where

$$V_i(s)=\frac{1}{16\pi}\left\{\varphi_i(s)-\frac{(M-m_i)^2}{s}[\varphi_i(s)-\varphi_i(0)]\right\},$$

$$i=1,2 \quad (A3)$$

and

$$\varphi_i(s)=(1/\pi)r_i\ln z_i,$$

$$r_i=\{[s-(M+m_i)^2]/[s-(M-m_i)^2]\}^{1/2}, \quad (A4)$$

$$z_i=(r_i+1)/(r_i-1).$$

W_1 and W_2 are, of course, related to the first and second channels, respectively. We shall henceforth drop the suffices wherever both channels are implied. The cuts of W in the s plane are determined by the cuts of φ. To find these we must define the branches of r and $\ln z$. If

$$\theta_1=\tan^{-1}\left[\frac{\mathrm{Im}\,s}{\mathrm{Re}\,s-(M-m)^2}\right],$$

$$\theta_2=\tan^{-1}\left[\frac{\mathrm{Im}\,s}{\mathrm{Re}\,s-(M+m)^2}\right],$$

$$(A5)$$

[7] W. R. Frazer and A. W. Hendry, Phys. Rev. 134, B1307 (1964).

then

$$r = |r| \exp[i(\theta_2 - \theta_1)]/2 \qquad \text{(A6)}$$

and the Riemann surface of r can be specified as follows:

$$\begin{aligned}
\text{sheet 1:} \quad & 0 < \theta_1 < 2\pi, \\
& -\pi < \theta_2 < \pi, \\
\text{sheet 2:} \quad & 2\pi < \theta_1 < 4\pi, \qquad \text{(A7)} \\
& -\pi < \theta_2 < \pi.
\end{aligned}$$

The cuts of $\ln z$ in the z plane are taken to the left. These definitions specify the analytic properties of φ, whose sheet we can describe in the following manner:

$$\begin{aligned}
\text{sheet A:} \quad & r \text{ on sheet } 1, \\
& -\pi < \arg z < \pi, \\
\text{sheet B:} \quad & r \text{ on sheet } 2, \\
& -3\pi < \arg z < -\pi, \qquad \text{(A8)} \\
\text{sheet C:} \quad & r \text{ on sheet } 2, \\
& \pi < \arg z < 3\pi, \text{ etc.}
\end{aligned}$$

There are, of course, an infinite number of sheets due to the infinity of sheets from the logarithm.

One can also show that the various sheets have the following cuts connecting the Riemann surface. Sheet A has only one cut to the right starting at $(M+m)^2$. The sheet reached by going through this cut is sheet B, but B also has a cut to the left starting at $(M-m)^2$ and in passing through this cut sheet C is reached. However, C has a right-hand cut as well, and this leads again to further sheets, and so on. Thus, of the infinite number of sheets of φ, one has a single right-hand cut, while all other sheets have both left- and right-hand cuts. It follows from the definition of W that the locations of the cuts of W are exactly the same as those of φ, and therefore the sheets of W may be described similarly to those of φ.

Finally, the physical singularities of D, which specify the unitarity cuts of the scattering amplitudes, can be deduced. The physical sheet must contain only right-hand cuts in D, so the physical sheet (or sheet I) of the scattering amplitudes is defined by taking W_1 and W_2 on their sheets A, which we shall designate by sheet A_1 and sheet A_2, respectively. Thus, the physical cut for T_{11}, for example, starts at s_1 due to the discontinuity in W_1, but there is an additional contribution starting at s_2 from the discontinuity in W_2. If one passes through the physical cut between s_1 and s_2, one arrives on a sheet which can be described by evaluating W_1 on sheet B_1 and W_2 on sheet A_2. We denote this sheet as sheet II. By going through the physical cut on sheet I above s_2, one can reach a sheet where W_1 is evaluated on sheet B_1 and W_2 on sheet B_2. This we designate sheet III. Finally, one can cross through the cut on sheet III between s_1 and s_2 and arrive on sheet IV, where W_1 is taken on sheet A_1 and W_2 on sheet B_2. The unphysical sheets II, III, and IV will also contain left-hand cuts which will lead to further sheets, but these four sheets
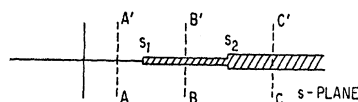
FIG. 10. The physical, or unitarity, cut on the physical sheet (sheet I). Below is shown a cross-sectional view of the unitarity cut and the sheets it connects.
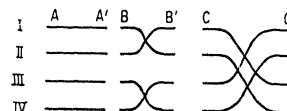
are those which are most intimately connected to the physical region and therefore of greatest interest as far as studying the effects of nearby singularities on the physical cross sections are concerned.

In Fig. 10, we show the physical cut on sheet I and also a cross-sectional view of this cut to illustrate how the four sheets are connected. We note that the point s_2 is common to all four sheets. Any unitarity preserving model of two-channel processes will contain sheets equivalent to these.[7]

The fourth quadrants of the four sheets and the singularities they contain in the single pole approximation are given in Fig. 11. Since Schwarz reflection applies to the scattering amplitudes, there is symmetry about the real axis. As the residue of the interaction pole is varied, poles of the scattering amplitude move about in unphysical regions as indicated in Fig. 11. The region about s_2 is noticeably bare of poles on all four sheets unlike the case of Frazer and Hendry, where a pole moving about s_2 was of prime importance to their
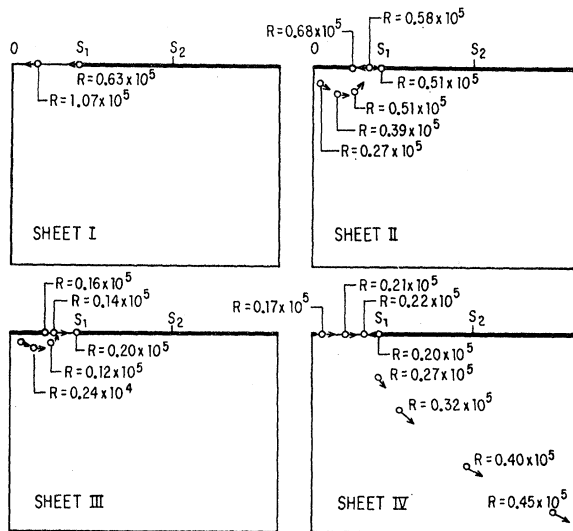
FIG. 11. The fourth quadrants of sheets I–IV and the singularities they contain for various values of the residue of the interaction pole in the single-pole approximation. Poles are denoted by circles and cuts by heavy lines. The interaction pole position is at $s_0 = -500 \, \mu^2$.

results. The behavior shown in Fig. 8 can nevertheless be reconciled with this somewhat disturbing fact if we remember that both channels in our model are in S waves, while in the Frazer-Hendry model, the first channel is in a D wave. If we look in Fig. 9 at the single-channel contributions (given by the dashed lines) to $\text{Re}[(U_1-W_1)(U_2-W_2)]$, we see that each has the usual cusp-like behavior at its respective threshold. Since both curves represent S-wave behavior, they have largely the same character and magnitude about their thresholds, and the resultant product which enters into the two-channel solution is thus almost constant between s_1 and s_2. We emphasize that the shape of this curve is purely a threshold phenomenon and is independent of the poles in the scattering amplitudes. The

effect of poles, so to speak, is simply to amplify the surrounding kinematic behavior. Thus, a pole in the scattering amplitude near the s_1 to s_2 region will tend to stress the flat behavior which occurs in the D function.

We see, in fact, that there is a pole near this region for appropriate values of R corresponding to curves in Fig. 8; namely, on sheet II there is a pole which approaches the point s_1 and eventually emerges on sheet I as a bound state. Because of the flat nature of the curve in Fig. 9, this pole can strongly influence the whole region between s_1 and s_2 and eventually give rise to the uppermost curves of Fig. 8. The shape of the lower cusp-like curves of Fig. 8 is due mainly to the numerator of T_{11} given by $R^2(U_2-W_2)$, whose real part is plotted in Fig. 9.

Polarization of Recoil Protons in π±p Elastic Scattering Near 600 MeV*

RICHARD D. EANDI, THOMAS J. DEVLIN,† ROBERT W. KENNEY, PAUL G. McMANIGAL,‡
AND BURTON J. MOYER

Lawrence Radiation Laboratory, University of California, Berkeley, California

(Received 15 June 1964)

Angular distributions of recoil-proton polarization in elastic $\pi^\pm p$ scattering were measured at 523-, 572-, and 689-MeV incident pion kinetic energy. Polarization measurements were made by observing the azimuthal asymmetry in the subsequent scattering of recoil protons in large carbon-plate spark chambers. Typical strong variation of the polarization with pion scattering angle near the πp diffraction minima was observed. Since existing opinion favors a D_{13} resonance at 600 MeV, a phase-shift analysis was attempted in order to confirm the existence and parity of this resonance. Available πp total and differential cross sections, these polarization data, and some possible restrictive assumptions related to the 600-MeV resonance were used in the analysis. Though the polarization results aided significantly in restricting the number of acceptable phase-shift sets, still, many plausible and qualitatively different sets were found.

I. INTRODUCTION

PRESENT knowledge of the natures of the various maxima occuring in the pion-nucleon cross sections,[1,2] for pion kinetic energies below 1.6 BeV (lab), includes quite certain assignments of angular momenta. Parities are, however, not confidently understood except in the well-known case of the "P_{33}" resonance (isotopic spin $T=\frac{3}{2}$, angular momentum $J=\frac{3}{2}$), occurring in pion scattering at 200-MeV kinetic energy in the laboratory frame, or 1238-MeV total energy in the πN center-of-mass frame.

Angular distribution in photoproduction[3–5] and in

elastic scattering[6,7] have allowed assignments of angular momentum to the phenomena here of interest as follows[8]:

Isotopic spin	Pion K. E. (Lab)	πN total c.m. energy	J
3/2	200 MeV	1238 MeV	3/2
1/2	600 MeV	1512 MeV	3/2
1/2	900 MeV	1688 MeV	5/2
3/2	1350 MeV	1920 MeV	7/2.

Our particular concern in this article is the phenomenon at 1512-MeV c.m. energy. Angular distribution measurements[8] infer that a $J=\frac{3}{2}$ amplitude is strong at this energy; but other amplitudes are not

[1] J. C. Brisson, J. F. Detoeuf, P. Falk-Vairant, L. van Rossum, and G. Valladas, Nuovo Cimento 19, 210 (1961).
[2] Thomas J. Devlin, Burton J. Moyer, and Victor Perez-Mendez, Phys. Rev. 125, 690 (1962).
[3] Ronald F. Peierls, Phys. Rev. 118, 325 (1960).
[4] F. P. Dixon and R. L. Walker, Phys. Rev. Letters 1, 458 (1958).

[5] J. I. Vette, Phys. Rev. 111, 622 (1958).
[6] Burton J. Moyer, Rev. Mod. Phys. 33, 367 (1961).
[7] Jerome A. Helland, Thomas J. Devlin, Donald E. Hagge, Michael J. Longo, Burton J. Moyer, and Calvin D. Wood, Phys. Rev. Letters 10, 27 (1963).
[8] Jerome A. Helland, Calvin D. Wood, Thomas J. Devlin, Donald E. Hagge, Michael J. Longo, Burton J. Moyer, and Victor Perez-Mendez, Phys. Rev. 134, B1079 (1964); Jerome A. Helland, Thomas J. Devlin, Donald E. Hagge, Michael J. Longo, Burton J. Moyer and Calvin D. Wood, ibid., 134, B1062 (1964).